Structure of ^{13}Be probed via secondary-beam reactions

G. Randisi,[1,*] A. Leprince,[1] H. Al Falou,[1,†] N. A. Orr,[1] F. M. Marqués,[1] N. L. Achouri,[1] J.-C. Angélique,[1] N. Ashwood,[2] B. Bastin,[1,‡] T. Bloxham,[2] B. A. Brown,[3] W. N. Catford,[4] N. Curtis,[2] F. Delaunay,[1] M. Freer,[2] E. de Góes Brennand,[5] P. Haigh,[2] F. Hanappe,[5] C. Harlin,[4] B. Laurent,[1,§] J.-L. Lecouey,[1] A. Ninane,[6] N. Patterson,[4] D. Price,[2] L. Stuttgé,[7] and J. S. Thomas[4,‖]

[1]*LPC-ENSICAEN, IN2P3-CNRS et Université de Caen, 14050 Caen Cedex, France*

[2]*School of Physics and Astronomy, University of Birmingham, Birmingham B15 2TT, UK*

[3]*NSCL and Department of Physics and Astronomy, Michigan State University, East Lansing, Michigan 48824, USA*

[4]*Department of Physics, University of Surrey, Guildford GU2 7XH, UK*

[5]*PNTPM, CP-229, Université Libre de Bruxelles, B-1050 Brussels, Belgium*

[6]*Slashdev Integrated Systems Solutions, B-5030 Gembloux, Belgium*

[7]*IPHC, Université Louis Pasteur et IN2P3-CNRS, 67037 Strasbourg Cedex 02, France*

(Received 26 November 2013; revised manuscript received 31 January 2014; published 26 March 2014)

The low-lying level structure of the unbound neutron-rich nucleus ^{13}Be has been investigated via breakup on a carbon target of secondary beams of ^{14,15}B at 35 MeV/nucleon. The coincident detection of the beam velocity ^{12}Be fragments and neutrons permitted the invariant mass of the $^{12}\mathrm{Be}+n$ and $^{12}\mathrm{Be}+n+n$ systems to be reconstructed. In the case of the breakup of ^{15}B, a very narrow structure at threshold was observed in the $^{12}\mathrm{Be}+n$ channel. Analysis of the $^{12}\mathrm{Be}+n+n$ events demonstrated that this resulted from the sequential decay of the unbound $^{14}\mathrm{Be}(2^+)$ state rather than a strongly interacting s-wave virtual state in ^{13}Be, as had been surmised in stable beam fragmentation studies. Single-proton removal from ^{14}B was found to populate a broad low-lying structure some 0.7 MeV above the neutron-decay threshold, in addition to a less prominent feature at around 2.4 MeV. Based on the selectivity of the reaction and a comparison with $(0-3)\hbar\omega$ shell-model calculations, the low-lying structure is concluded to arise from closely spaced $J^\pi = 1/2^+$ and $5/2^+$ resonances ($E_r = 0.40 \pm 0.03$ and $0.85^{+0.15}_{-0.11}$ MeV), while the broad higher-lying feature is a second $5/2^+$ level ($E_r = 2.35 \pm 0.14$ MeV). Taken in conjunction with earlier studies, the results suggest that the lowest $1/2^+$ and $1/2^-$ levels lie relatively close together below 1 MeV.

DOI: 10.1103/PhysRevC.89.034320 PACS number(s): 27.20.+n, 25.60.Gc, 25.90.+k

I. INTRODUCTION

Light nuclei have long provided a test bench for our understanding of nuclear structure. Indeed, one of the central themes of present-day studies—the evolution of shell structure with isospin—may arguably be traced back to the seminal work of Talmi and Unna on the ordering of the $\nu 2s_{1/2}$–$\nu 1p_{1/2}$ levels in ^{11}Be [1]. With the advent of radioactive beams it has become possible to explore experimentally isotopic chains in the light mass region to the very limits of stability and beyond, thus providing for more stringent tests of nuclear structure models.

In this context the beryllium isotopes are of particular interest, as they exhibit a rich variety of structural phenomena, ranging from the α clustering of ^{8}Be and the deformed 2α-Xn "molecular" character of ^{9,10}Be [2,3], through the single-neutron halo of ^{11}Be [4] and the breakdown of the $N = 8$ p-shell closure of ^{12}Be [5–7], to the Borromean two-neutron halo of ^{14}Be [8–10]. The $N = 9$ member of the Be isotopic chain, ^{13}Be, which is neutron unbound [11,12], thus presents an intriguing study. First, in terms of the halo of ^{14}Be, the level structure of ^{13}Be is critical in establishing the $^{12}\mathrm{Be}+n$ interaction, an essential component in three-body modeling [13,14]. Second, from a structural point of view, the dominant $\nu 2s_{1/2}$ ground-state configurations of the less exotic $N = 9$ isotones ^{14}B [15–18] and ^{15}C [16,17,19] suggest that the lowering of the $\nu 2s_{1/2}$ single-particle orbital with respect to the $\nu 1d_{5/2}$ responsible for this [1,20] may well also generate an inversion of the $1/2^+$ and $5/2^+$ levels in ^{13}Be. Such behavior, while in line with the dominant $2s^2_{1/2}$ valence neutron structure of ^{14}Be [21–23], is complicated by the deformed [24] mixed $(0+2)\hbar\omega$ character of ^{12}Be [5–7], which, as posited by some models [25–27], would suggest that there is also a low-lying $1/2^-$ state in ^{13}Be. In the work presented here, we concentrate on locating the $\nu 2s_{1/2}$ and $\nu 1d_{5/2}$ levels and determining the character of the former.

Beginning with the first indication of an unbound resonance, lying around 1.8 MeV above the $^{12}\mathrm{Be}+n$ threshold (width $\Gamma = 0.9 \pm 0.5$ MeV) [28], ^{13}Be has been the object of a range of measurements employing both stable [28–32] and radioactive [22,33–37] beams, including pion absorption [38]. The heavy-ion multinucleon transfer studies all agree on the existence of a well-defined resonance around 2 MeV above the $^{12}\mathrm{Be}+n$ threshold [28–30], the intrinsic width ($\Gamma \approx 0.3$ MeV) of which is compatible with an $\ell = 1$ or 2 assignment [29]. Strong arguments for a $5/2^+$ assignment were made based on the comparison of the (^{11}B,^{12}N) reaction on ^{12}C and ^{14}C, leading to ^{11}Be and ^{13}Be, whereby the

*Present address: Instituut voor Kern- en Stralingsfysica, KU Leuven, B-3001 Leuven, Belgium.

†Present address: Université de Technologie et de Sciences Appliquées Libano-Française, Tripoli, Lebanon.

‡Present address: GANIL, Caen, France.

§Present address: CEA, DAM, DIF, F-91297 Arpajon, France.

‖Present address: Schuster Laboratory, The University of Manchester, Manchester, UK.

well-known ^{11}Be 1.78-MeV $5/2^+_1$ state was the most strongly populated in the former case [30]. A weakly populated peak was also observed at 0.80 ± 0.09 MeV above threshold in ^{14}C(^{11}B,^{12}N), which, based again on comparison with the same reaction on ^{12}C, was tentatively assigned $J = 1/2$. It may be noted, however, that such heavy-ion multinucleon transfer reactions with very negative Q values do not favor low transferred angular momentum [39,40]. Indeed, as is well evidenced by attempts [41–43] to locate the now well-known threshold $\nu 2s_{1/2}$ state in ^{10}Li, it is extremely difficult to populate such states in this manner. In addition, given that stopped pion-absorption reactions do not appear to readily populate $\ell = 0$ states [44] and the preliminary report of a resonance 0.65 ± 0.10 MeV above threshold in the ^{14}C(π^-, p) reaction [38], it may be concluded that there is quite probably a $1/2^-$ level around 0.8 MeV above threshold. It is worthwhile noting that, as opposed to the ^{12}Be $+ n$ invariant mass studies, which can be influenced by bound excited states of the ^{12}Be fragment, missing mass measurements provide unambiguous determinations of the ^{13}Be energies.

Two other stable-beam studies have been undertaken in which the relative velocity spectra for ^{12}Be fragments and neutrons following fragmentation of beams of ^{18}O [31] and ^{48}Ca [32] were investigated. In both cases very narrow structures centered at zero were observed and interpreted as arising from a strongly interacting virtual s-wave state (scattering length $a_s < -10$ fm).

Turning to the radioactive-beam reaction studies, both proton and neutron removal (or "knockout") from ^{14}B [36] and ^{14}Be [22,34,37], respectively, have been investigated. The proton removal study by Lecouey [36], which reports our first efforts to study the C(^{14}B,^{12}Be $+ n$) reaction, observed, in the decay energy spectrum, a very broad structure ($\Gamma \approx 1.3$ MeV) centered some 0.7 MeV above threshold together with a narrower peak ($\Gamma \approx 0.4$ MeV) at around 2.4 MeV, which were identified, based on the selectivity of the reaction, as $1/2^+$ and $5/2^+$ resonances. Subsequent neutron-knockout studies [22,34,37] exhibited ^{12}Be $+ n$ invariant mass (or decay energy) spectra with a somewhat narrower low-lying structure at ∼0.5 MeV and a broader feature at around 2–3 MeV. At intermediate energies with a proton target and guided by the reconstructed ^{12}Be $+ n$ transverse momentum distributions, a p-wave resonance at 0.51 ± 0.10 MeV ($\Gamma = 0.45 \pm 0.3$ MeV) and a very broad ($\Gamma = 2.4 \pm 0.2$ MeV) d-wave structure were identified [34]. These features were superposed on an underlying distribution which was modeled as a very weakly interacting s-wave virtual state (scattering length $a_s \approx -3$ fm). At a high beam energy using a carbon target the interpretation was also guided by the ^{12}Be $+ n$ transverse momentum distributions as well as the ^{12}Be $- n$ angular correlations [22]. In this case, a more complex interpretation of the invariant mass spectrum was proposed, in which ^{13}Be states at 2.0 MeV (assigned $J^\pi = 5/2^+$) and 3.0 MeV ($1/2^-$) have neutron decay branches to ^{12}Be$^*(2^+_1,0^+_2,1^-_1)$. In addition, a significant contribution from a very weakly interacting s-wave virtual state ($a_s \approx -3$ fm) was postulated. Very recently, improved data recorded at very high beam energies using a proton target have been reported [37], and a detailed analysis, taking into account earlier studies (in particular, Refs. [34] and [36]), suggests that the decay energy spectrum is dominated by resonant s-wave strength, especially at a low decay energy, in addition to a $5/2^+$ state at 2.0 MeV and other possible weaker higher-lying states at around 3 and 5 MeV [45]. Finally, despite the relatively high background, an early investigation of the $d(^{12}\text{Be},p)$ transfer reaction also indicated the presence of a state at around 2 MeV [33].

From a theoretical point of view, approaches ranging from the shell model [34,46,47] to various few-body calculations [13,14,25,26,48–50], including deformation [51], together with the relativistic mean-field [52] and antisymmetrized molecular dynamics [27] models, have been employed to explore the structure of ^{13}Be. Apart from general agreement on the existence of a $\nu 1d_{5/2}$ resonance well removed from the ^{12}Be $+ n$ threshold, no systematic conclusions may be drawn regarding any lower-lying levels. It is interesting to note that the $5/2^+$ level, as observed in the ^{13}C(^{14}C,^{14}O)^{13}Be reaction at 2.01 ± 0.05 MeV, has served as a reference point, together with the constraint provided by the ^{14}Be binding energy, for the majority of the few-body calculations [13,25,48,49].

In the present paper we report on the investigation of ^{13}Be using single-proton removal from ^{14}B and breakup of ^{15}B at intermediate energies (35 MeV/nucleon). As argued elsewhere [53–56], proton removal presents the advantage of preferentially populating states whereby the neutron configuration remains little perturbed with respect to that of the projectile. As such, it is expected that by employing a ^{14}B beam here final states in ^{13}Be with $\nu 2s_{1/2}$ and $\nu 1d_{5/2}$ configurations should be preferentially populated [15–18]. In principle, breakup of ^{15}B, which involves proton and neutron removal, has the potential to populate a broader variety of states. However, as will be seen, the ^{12}Be $+ n$ channel is dominated by events of very low relative energy resulting from the in-flight decay of the unbound 2^+_1 state of ^{14}Be, which were interpreted in earlier stable-beam fragmentation experiments as arising from a strongly interacting threshold s-wave virtual state in ^{13}Be [31,32].

II. EXPERIMENT

The ^{14,15}B secondary beams with mean energies of 35 MeV/nucleon were produced via the reaction on a 3.1-mm-thick Be target of a 55 MeV/nucleon ^{18}O primary beam supplied by the GANIL coupled-cyclotron facility. The beam velocity reaction products were analyzed and purified using the LISE3 fragment separator employing an achromatic degrader [57]. Two separate settings of the separator were used for each of the beams so as to optimize the intensities (^{14}B, $\sim 1.3 \times 10^4$ pps; ^{15}B, $\sim 8 \times 10^3$ pps) and purities (>95%).

A time-of-flight measurement performed using the signal derived from the cyclotron radio frequency and a thin (100-μm-thick) plastic scintillator detector mounted just upstream of the first beam tracking detector (see below) allowed the ^{14,15}B ions to be easily separated from the remaining contaminants in the off-line analysis. The energy spread of the ^{14,15}B beams, as defined by the settings of the LISE spectrometer, was 1.5% ($\Delta E/E$). The effect on the relative

energy between the ^{12}Be fragment and the neutron from the in-flight decay of ^{13}Be was negligible compared to the overall resolution and no event-by-event correction based on the measured beam particle velocities was required.

The secondary beam was delivered onto a 190 mg/cm^2 ^{nat}C target. Owing to the limited optical qualities of the secondary beams (beam spot size, ∼10 mm in diameter), two position-sensitive drift chambers [58], located just upstream of the secondary reaction target and separated by 55 cm, were used for tracking. The fast timing signal provided by the thin scintillator detector was used as the timing reference for the drift chamber position measurements. The impact point of the beam on target was subsequently reconstructed event by event, with a resolution of ∼1.5 mm (FWHM).

The charged fragments from the reactions were detected and identified using a Si-Si-CsI(Tl) telescope centered at 0° downstream of the secondary target. The two 500-μm-thick (50×50 mm^2) silicon detectors, each comprising 16 resistive strips (3 mm wide), were mounted such that the strips of the first detector provided for a measurement of position in the vertical direction, while those of the second detector furnished the horizontal position determination. These detectors were located 15 cm downstream of the target, and the impact point along each strip was determined with a resolution of 1 mm (FWHM), significantly better than the individual strip width. In addition to the energy-loss measurements furnished by the silicon detectors, the residual energy of each fragment was determined from the signals derived from an array of sixteen $25 \times 25 \times 25$ mm^3 CsI(Tl) crystals which were located 30 cm downstream of the target so as to subtend the same solid angle as the Si detectors. The measurement of the total energy deposited in the telescope by the charged fragments was calibrated using a mixed secondary beam, which included ^{12}Be, and for which the energy spread was limited to 0.1%. A series of measurements was made over a range of rigidity settings of the LISE spectrometer such that the ^{12}Be calibration points covered the range of energies expected from the in-flight decay of ^{13}Be. The total energy resolution of the telescope was determined to be some 2% (FWHM) [59,60]. In addition to the measurements of breakup on the C target, data were also acquired with the target removed so as to ascertain the contribution arising from interactions in the telescope. As the reactions of interest involve charge changing with respect to the projectile, this contribution was found to be negligible, as expected [61].

The neutrons were detected using 90 elements of the DEMON liquid scintillator detector array [62,63]. The use of such an array enabled the ambient γ-ray background to be eliminated using pulse-shape discrimination (prompt-reaction-induced γ rays can also be rejected using the time of flight), allowing, importantly, a very low threshold on the deposited energy (500 keVee) to be imposed, thus maximizing the efficiency, rather than the ∼6 MeVee required to otherwise veto such events. The intrinsic detection efficiency of each module was ∼35% at 35 MeV [64]. The overall time-of-flight resolution, including the contribution of the thin plastic start detector, was 1.5 ns (FWHM).

As in previous experiments [7,21,35,36,65], the array was arranged in a staggered multiwall-type (or "zigzag") configuration [66] covering polar angles up to 27° in the laboratory frame [59,67].[1] This arrangement provided for a good detection efficiency for the ^{12}Be + n reaction channel out to ∼5 MeV relative energy (Fig. 1) and good granularity—the angular resolution in the neutron detection[2] being the major contribution to the final reconstructed ^{12}Be + n decay energy resolution (Fig. 1) [67]. This configuration was also optimized to provide, in the case of multineutron detection (here ^{12}Be + n + n), for the rejection of cross talk (events arising from the scattering of a neutron from one detector into another, with the deposited energy registered above threshold in both) in the off-line analysis using kinematic considerations coupled with the energy deposited in the modules [66]. Finally, it may be noted that the rate of events for which a neutron was first scattered without detection by a module (or nonactive element in the setup) and then detected in another module was estimated, via simulations, to be considerably less than 5% of the total number of ^{12}Be + n events and produced negligible distortions in the reconstructed decay energy spectra, as further confirmed by the measurement of the ^{7}He ground state (see below).

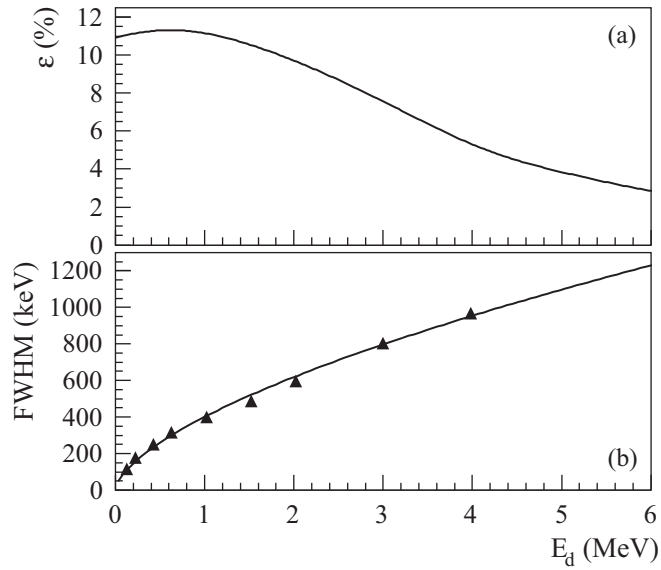

FIG. 1. (a) Simulated efficiency for the detection of ^{12}Be + n pairs as a function of decay energy (E_d). (b) Simulated resolution of the reconstructed ^{12}Be + n decay energy.

The neutron velocity was derived from the time of flight measured between the thin plastic scintillator detector and the DEMON module(s) which registered an event. The neutron energy spectra were dominated by beam velocity neutrons produced in the projectile breakup; the relatively weak low-energy component arising from neutrons evaporated from the target was removed in the off-line analysis by imposing a low-energy threshold of 11 MeV [59,60] (Fig. 3).

[1]The single-wall configuration presented in the review of Ref. [68] was only utilized in the very first radioactive-beam experiment employing DEMON [61].

[2]Ranging from 1.4° to 2.6°, depending on the distance of the module from the target.

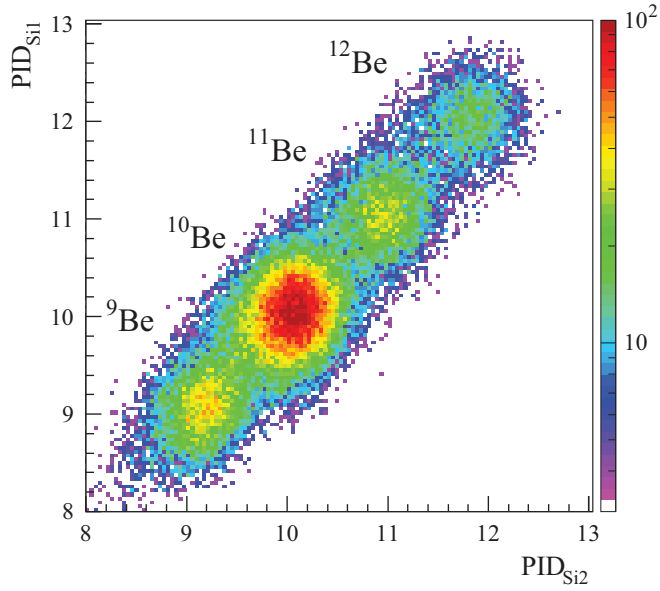

FIG. 2. (Color online) Particle identification (PID) derived from the Si-Si-CsI detector telescope for the beryllium isotopes in coincidence with beam velocity neutrons for the C(^{14}B,^{A}Be + n) reaction (see text).

III. RESULTS

The identification of the beryllium fragments in coincidence with fast neutrons ($E_n > 11$ MeV) is shown in Fig. 2, where two particle-identification parameters (PIDs) were constituted using the energy losses from each of the two silicon detectors together with the residual energy derived from the CsI(Tl) crystals [67]. As may be seen, the ^{12}Be fragments are clearly separated from the more prolific lighter mass isotopes. Furthermore, as expected, the neutrons detected in coincidence with the ^{12}Be fragments exhibit energies centered around 35 MeV (Fig. 3).

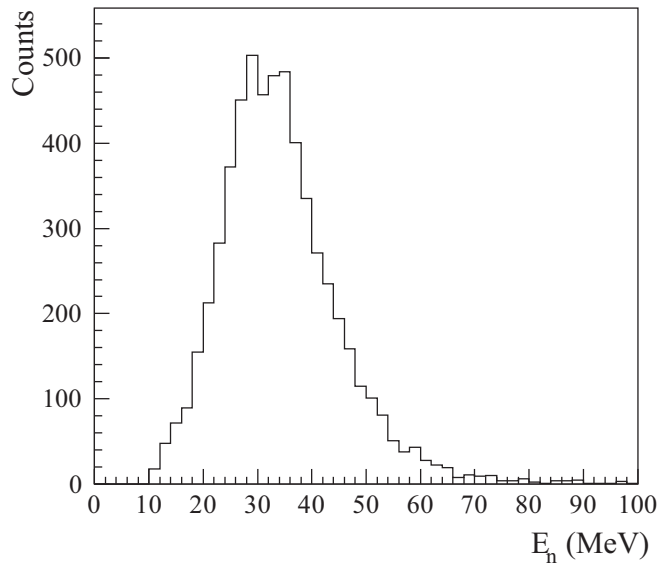

FIG. 3. Neutron energy spectrum for events with $E_n > 11$ MeV detected for the C(^{14}B,^{12}Be + n) reaction.

The decay (or relative) energy E_d was derived from the measured four-momenta of the ^{12}Be fragment and neutron,

$$E_d = M_{\text{inv}} - (m_f + m_n), \tag{1}$$

where m_f and m_n are the masses of the charged fragment and the neutron, respectively, and the invariant mass M_{inv} is given by

$$M_{\text{inv}}^2 = (\epsilon_f + \epsilon_n)^2 - (\vec{p}_f + \vec{p}_n)^2, \tag{2}$$

where ϵ_f and ϵ_n are the total (kinetic and rest mass) energies of the fragment and neutron.

Given the complex nature of the setup employed here, careful attention was paid, as in previous experiments of this type which we have carried out [7,21,55,56,69], to understand its effects, in particular, on the reconstructed decay energy. To do so a detailed simulation which took into account the characteristics (resolution, intrinsic efficiency and geometry) of all the detectors, as well as the beam characteristics and the effects of the target and the reaction, was developed. Owing to the granular character of the neutron-detection array, an important element in correctly describing the response of the setup is, as noted in our earlier work [55,67], the transverse momentum distribution of the decaying neutron unbound system—here ^{13}Be. The intrinsic widths of the ^{13}Be transverse momentum distributions for both the C(^{14}B,^{12}Be + n) and the C(^{15}B,^{12}Be + n) reactions were thus adjusted within the simulations such that they matched the experimental widths (300 and 340 MeV/c FWHM, respectively) reconstructed from the measured momenta of the ^{12}Be fragment and neutron [59,60]. Importantly, the simulations were benchmarked not only against codes developed independently as part of earlier work [67,69] but also through the ability to reproduce the well-known ^{7}He $3/2^-$ ground-state resonance [70], which was populated here in the C(^{14,15}B,^{6}He + n) reactions [59,60] (Fig. 4).

The results of the simulations for the response of the setup for the C(^{14}B,^{12}Be + n) reaction are displayed in Fig. 1 as a function of the decay energy. Very similar behavior was found for the C(^{15}B,^{12}Be + Xn) reactions, except for the overall detection efficiency (ε), which was lower by a factor of 10 for the two-neutron channel [60]. The predicted efficiency for detecting a ^{12}Be + n pair is shown in Fig. 1(a). Importantly, the response is a smooth function of the decay energy, exhibiting no features which could mimic a resonance-like state. The gradual falloff from a maximum of some 12% at around 1 MeV is in line with simple geometrical considerations based on the angular coverage of the neutron array (the efficiency for the detection of ^{12}Be fragments is essentially 100%). The resolution of the reconstructed decay energy, which is dominated by the finite angular size of the individual DEMON modules, was determined to vary as $0.40\sqrt{E_d}$ MeV [Fig. 1(b)], with, for example, a resolution of close to 330 keV expected at 0.7 MeV. It may be noted that, owing to the slow falloff in the detection efficiency with decay energy, the apparent position of peaks are slightly downshifted in energy for E_d above 1 MeV [59].

As described in our earlier work, in addition to the events arising from fragment + neutron final-state interactions associated with the decay of the unbound states, care must be taken to account for uncorrelated events [55,56,67,69]. Such events may arise from a number of sources. In reactions involving proton-only removal, such as C(^{17}C,^{15}B + n) [55,67] or, here, C(^{14}B,^{12}Be + n), the nonresonant continuum may be populated via the fragment recoil effect [54] and scattering of the weakly bound projectile valence neutron by the target.[3] In the case of breakup, whereby the outgoing channel of interest has fewer neutrons than the projectile—here C(^{15}B,^{12}Be + n) and C(^{14}B,^{6}He + n)—an additional contribution arising from the detection of a neutron(s) that does(do) not correspond to the population of fragment + neutron states will also be present. As discussed in detail and demonstrated in Refs. [55] and [67], the distribution of uncorrelated events may be estimated by event mixing using the measured fragment + neutron pairs, provided that care is taken to eliminate the effects of any "residual" correlations arising from the resonant structures themselves [65]. Importantly, this technique involves no *ad hoc* assumptions or parametrizations and the distribution so obtained incorporates explicitly the effects of the experimental response. As such, it may be compared directly with the measured distribution in order to identify features arising from final-state interactions associated with the decay of unbound states [67].

[3]In practice, given the limited resolution and decreasing detection efficiency at high decay energies, events corresponding to very broad, weakly populated levels may also contribute.

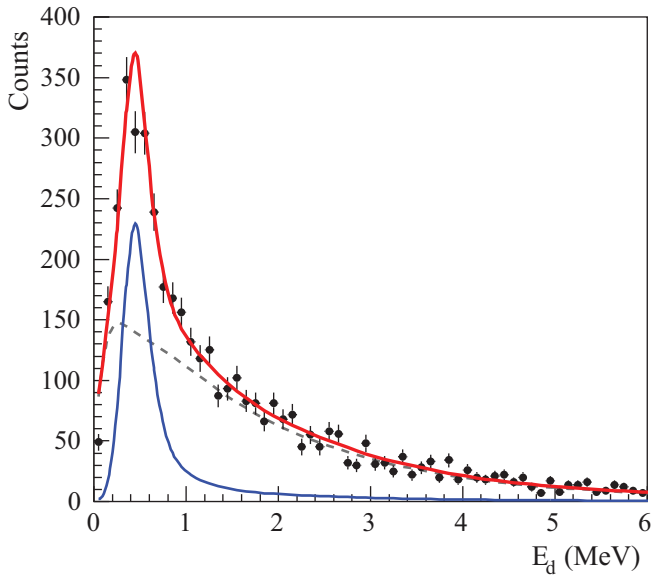

FIG. 4. (Color online) Reconstructed ^{6}He + n decay energy for the C(^{14}B,^{6}He + n) reaction. Results of a fit using the simulated line shape for the known ^{7}He $3/2^-$ ground-state resonance [lower (blue) solid line], together with an uncorrelated distribution generated by event mixing [dashed (gray) line; see text].

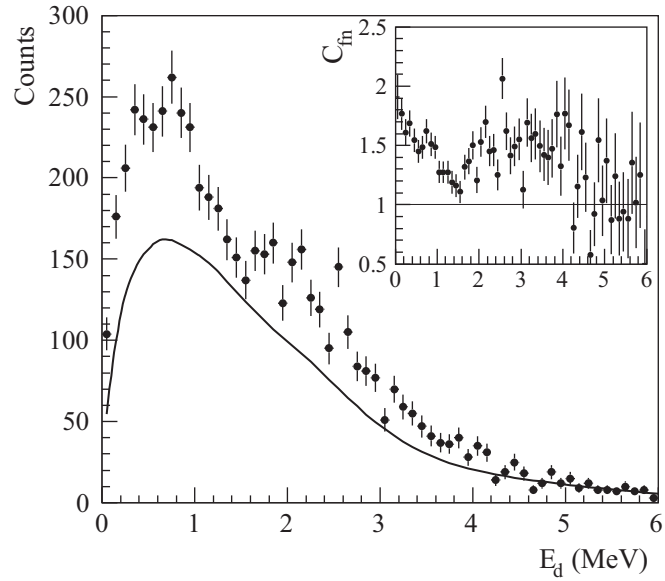

FIG. 5. Reconstructed ^{12}Be + n decay energy for the C(^{14}B, ^{12}Be + n) reaction compared to the uncorrelated distribution (solid line; see text) normalized to the region above 4 MeV. Inset: ^{12}Be + n correlation function, $C_{\rm fn}$ (see text).

Assuming that the form of the event-mixed distribution provides a good description of the uncorrelated events (and, in practice, this appears to be the case [55,56,67,69]), the overall contribution to the decay energy spectrum must be determined. In the following, as in our earlier studies, the contribution of the uncorrelated distribution to the invariant mass spectrum was allowed to vary within the fitting procedures used to derive the final results and associated uncertainties. In addition, based on these fits, the ability to reproduce other observables, such as the ^{12}Be + n momentum distributions and the neutron energy spectrum, was verified [59,60].

A. The C(^{14}B,^{12}Be + n) reaction

The reconstructed decay energy spectrum obtained for the C(^{14}B,^{12}Be + n) reaction is shown in Fig. 5. For comparison, the uncorrelated distribution, obtained via event mixing and normalized to the region above 4 MeV, is included. It is clear that structures corresponding to ^{12}Be + n final-state interactions are present at ∼1 MeV and below, as well as in the region around 2–3 MeV. This is even more apparent in the inset in Fig. 5, whereby the ^{12}Be + n correlation function, $C_{\rm fn}$, obtained as the ratio of the measured to the uncorrelated distributions, is displayed.

Before attempting to interpret the ^{12}Be + n decay energy spectrum, the issue of bound excited states of ^{12}Be should be addressed. At present, ^{12}Be is known to have three bound excited states: the well-established 2^+_1 state at 2.11 MeV [71], together with a 1^- state at 2.7 MeV [24] and an isomeric 0^+_2 level ($\tau_{1/2} \approx 300$ ns) at 2.25 MeV [72,73]. The population of any of these levels will, as alluded to in Sec. I, provide for ambiguities in the interpretation of the ^{12}Be + n coincidences. For example, if a level in ^{13}Be lying 2.30 MeV above the ^{12}Be + n decay threshold were to have an appreciable

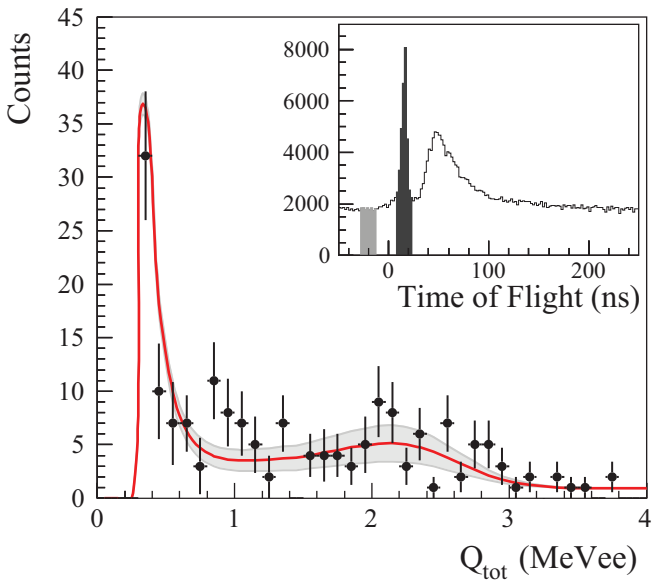

FIG. 6. (Color online) Total charge (Q_{tot}) spectrum for prompt γ rays recorded in DEMON in coincidence with ^{12}Be fragments for the C(^{14}B,^{12}Be) reaction. The line and shaded band represent the best fit ($5 \pm 2\%$) for the simulated line shape for 2.1-MeV γ rays emitted from the in-flight decay of ^{12}Be(2^+_1). Inset: Time of flight for events identified as γ rays (see text). Prompt reaction γ rays are identified by the black-shaded peak. The contribution from random coincidences with ambient γ rays was estimated, as shown by the gray-shaded region.

branching ratio for decay to ^{12}Be(2^+_1) + n, then the ^{12}Be + n decay energy spectrum would exhibit, in addition to a peak at 2.30 MeV, another near threshold ($E_d = 0.19$ MeV). In the present experiment, no dedicated γ detection was available. It was possible, however, to obtain an estimate of the percentage of ^{12}Be fragments in bound excited states (other than the isomeric state) using the DEMON array.

Specifically, events corresponding to γ rays were selected using the pulse-shape discrimination capability of DEMON. Prompt reaction γ rays were then isolated by their time of flight and an estimate was made of the small number of underlying random events [inset in Fig. 6, where, for clarity, the time of flight is shown for C(^{14}B, fragment + γ)]. The energy, or total charge (Q_{tot}), deposited in the detector modules was carefully calibrated using γ-ray sources, and as such, the form of the Compton edge and overall response to γ rays, including the resolution, was well established [59]. In order to provide for a comparison with the data, a simulation was employed to take into account the Doppler shift as well as the intrinsic and geometric efficiency of the array for the moving source ($\varepsilon_\gamma = 0.07\%$) [59]. Owing to the very limited efficiency for ^{12}Be + n + γ triple coincidences ($\sim$0.007%), only ^{12}Be + γ coincidences could be examined here. The results are displayed in Fig. 6, where the simulated line shape expected for the decay of ^{12}Be(2^+_1) is shown. The same analysis was also performed for the C(^{14}B,^{6}He + γ) reaction [59], whereby, owing to the lack of any bound ^{6}He excited states, no events are expected from a beam velocity source. This allowed the small background of events in the region of Q_{tot} expected for ^{12}Be* γ decays to be determined and the shape of the fast-rising peak of events at threshold to be verified. The best-fit estimate of the percentage of excited ^{12}Be(2^+_1) fragments was $5 \pm 2\%$, with no discernible population of ^{12}Be(1^-). This result is in line with a measurement made using a set of small NaI detectors with a low efficiency in our preliminary study of C(^{14}B,^{12}Be + n) [67]. As such, excluding the possible population of the isomeric 0^+_2 level (Sec. V), to which the above analysis is insensitive, the following discussion considers that the C(^{14}B,^{12}Be + n) reaction proceeds via the ^{12}Be ground state.

Returning to the interpretation of the C(^{14}B,^{12}Be + n) decay energy spectrum, we proceed by assuming, as outlined in Sec. I, that the removal of a proton leaves the projectile neutron configuration intact [53–56]. Given that the ^{14}B valence neutron configuration is dominated by $\nu 2s_{1/2}$ and $\nu 1d_{5/2}$ components [15–18]—$C^2S(^{13}\mathrm{B}_{gs}(3/2^-) \otimes \nu n\ell j) = 0.65$ and 0.31, respectively [15–17]—states with the corresponding neutron configurations are expected to be populated in ^{13}Be.

In order to generate the line shapes needed to interpret the ^{12}Be + n decay energy spectrum, the relatively simple approach developed in Refs [53,54], and [74] has, as in our earlier work [36,55,56], been followed. That is, the line shape of the fragment − neutron relative energy distribution was derived from the overlap of the initial bound-state wave function, describing the relative motion between the valence neutron, $\nu n\ell j$, and the ^{13}B core of the ^{14}B projectile and the unbound final-state wave function describing the ^{12}Be − neutron interaction (thus neglecting the momentum transfer). As detailed in Refs. [67] and [75], for a resonance, this approach results in a line shape essentially identical to that of the single-level R-matrix approximation.[4] As such, R-matrix line shapes were employed [76], whereby the width is dependent on the energy and ℓ through the penetrability coefficients, and $\Gamma(E_d) = \Gamma_r P_\ell(E_d)/P_\ell(E_r)$, where Γ_r is the width at $E_d = E_r$ [77].

In the case of an s-wave virtual state, the asymptotic behavior of the bound $\ell = 0$ initial-state wave function was described by Hankel functions, with decay length $\alpha = \sqrt{2\mu_{13-n} S_n}/\hbar$ (where μ_{13-n} is the ^{13}B − n reduced mass and S_n is the ^{14}B single-neutron binding energy of 0.97 MeV). The asymptotic form of the unbound final state was taken as a linear combination of spherical Bessel and Neumann functions, characterised by the ^{12}Be − n relative wave number $k = \sqrt{2\mu_{12-n} E_d}/\hbar$ (where μ_{12-n} is the ^{12}Be − n reduced mass) [59,67]. A general solution for the unbound scattering state was obtained by matching the logarithmic derivative of the asymptotic solution (valid in the region external to the potential) and a numerical solution obtained for the internal region [78]. The scattering length (a_s), which describes the strength of the fragment-neutron final-state interaction in the s-wave channel, is related to the phase shift (δ_0) as $a_s = -\lim_{k\to 0} \frac{d\delta_0}{dk}$. From a practical point of view it is important to note that, except for values of a_s close to zero, the line shape

[4] As such, possible interference between resonances of the same spin-parity is not considered here.

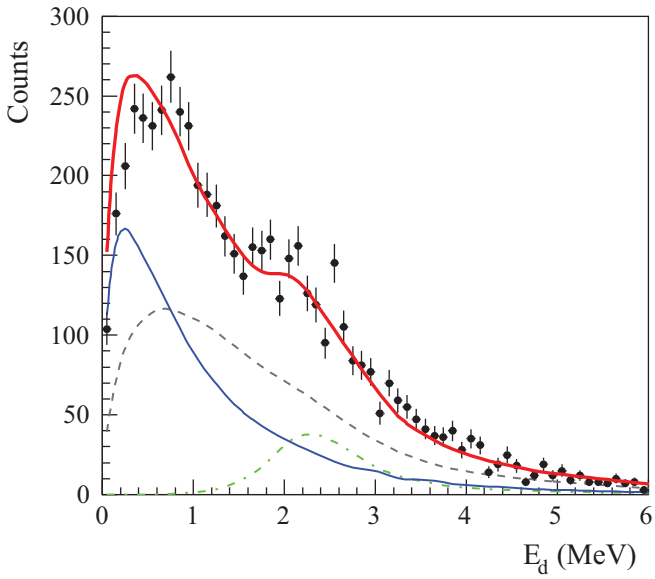

FIG. 7. (Color online) Reconstructed ^{12}Be + n decay energy for the C(^{14}B,^{12}Be + n) reaction compared to simulations incorporating an s-wave virtual state [lower (blue) solid line], a higher-lying d-wave resonance [dot-dashed (green) line], and a nonresonant continuum [dashed (gray) line] (see text).

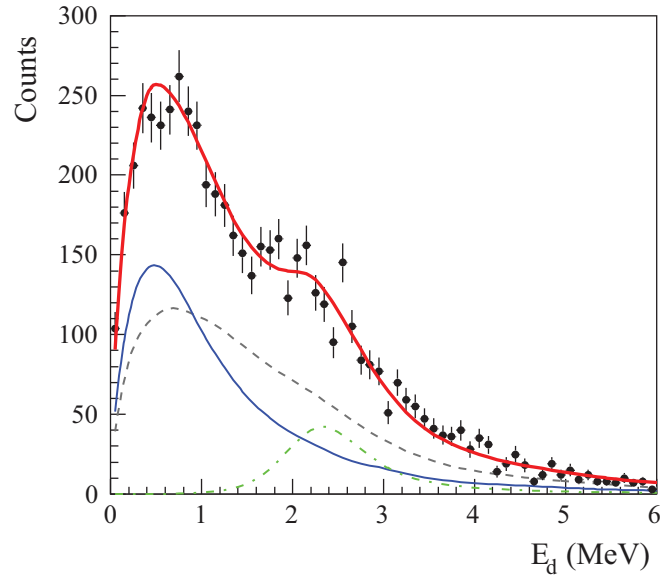

FIG. 8. (Color online) Reconstructed ^{12}Be + n decay energy for the C(^{14}B,^{12}Be + n) reaction compared to simulations incorporating an s-wave resonance [lower (blue) solid line], a higher-lying d-wave resonance [dot-dashed (green) line], and a nonresonant continuum [dashed (gray) line] (see text).

characteristically rises very quickly at very low E_d, then falls off with a gradual decay towards higher energies [67,75].

Assuming that the relative strengths of the s- and d-wave states in ^{13}Be reflect those of the parent configurations in ^{14}B, and given that any s-wave state well away from threshold will be extremely broad and consequently difficult to distinguish, the ^{12}Be + n decay energy spectrum was described in the first instance by a near-threshold virtual s-wave state, a higher-lying d-wave resonance, and the uncorrelated distribution. Apart from the latter (see above), the theoretical line shapes were used as input to the Monte Carlo simulation of the experiments. The scattering length, resonance energy and width, and intensities of each of the three distributions were left as free parameters. The best fit to the data is displayed in Fig. 7, where a lower limit on the scattering length of $a_s = -3$ fm could be determined and the resonance parameters of the the higher-lying feature were deduced to be $E_r = 2.40 \pm 0.20$ MeV and $\Gamma_r = 0.90 \pm 0.22$ MeV. While the spectrum is well described above 1.5 MeV, the theoretical distribution in the lower region rises too quickly at threshold and peaks 0.3 MeV below the data. As in our preliminary work [36], diminishing, or even eliminating completely, the contribution from the uncorrelated events degrades further the agreement with the data. It may also be noted that an even worse description of the data is obtained if the very strongly interacting virtual s state ($a_s < -10$ fm) posited in the stable-beam fragmentation experiments is employed [31,32]. We return to this in the following section.

At this juncture it is worth recalling that the conditions required for the formation of a virtual s-wave scattering state are quite specific; namely, the potential should be spherical and inert, with no internal degrees of freedom (as such, the scattering state will be, by definition, pure s wave). Given that ^{12}Be is known to be well deformed [24], the formation of resonances with $\ell_n = 0$ becomes possible [79,80]. Indeed, within the R-matrix approach resonances and virtual s states occur, depending on the character of the corresponding poles [76,81]. Thus, in the same vein as our preliminary study [36], a description of the ^{12}Be + n decay energy spectrum employing an s-wave resonance at low energy was attempted. Figure 8 displays the results, where a good agreement is obtained with the data for an s-wave resonance at 0.70 ± 0.11 MeV and $\Gamma_r = 1.70 \pm 0.22$ MeV, along with a d-wave resonance at 2.40 ± 0.14 MeV with $\Gamma_r = 0.70 \pm 0.32$ MeV. The uncertainties include not only those arising from the fitting, but also an estimate of effects arising from the calibrations (in particular, the absolute calibrations of the ^{12}Be and neutron momenta) and the construction of the uncorrelated distribution. In the context of the latter, it may be noted that the description of the data in the region below $\sim$1 MeV is rather poor if the uncorrelated distribution is eliminated [59].

B. The C(^{15}B,^{12}Be + n) reaction

The reconstructed decay energy spectrum for the C(^{15}B,^{12}Be + n) reaction is displayed in Fig. 9. The most striking aspect of the spectrum, which bears little resemblance to that obtained in proton removal from ^{14}B, is the very narrow, strongly populated peak at threshold. The removal of a proton and a neutron from ^{15}B may occur in two ways: (i) both particles are directly removed in a single step by the interaction with the target, or (ii) in the first step, proton removal populates continuum states in ^{14}Be which subsequently neutron decay

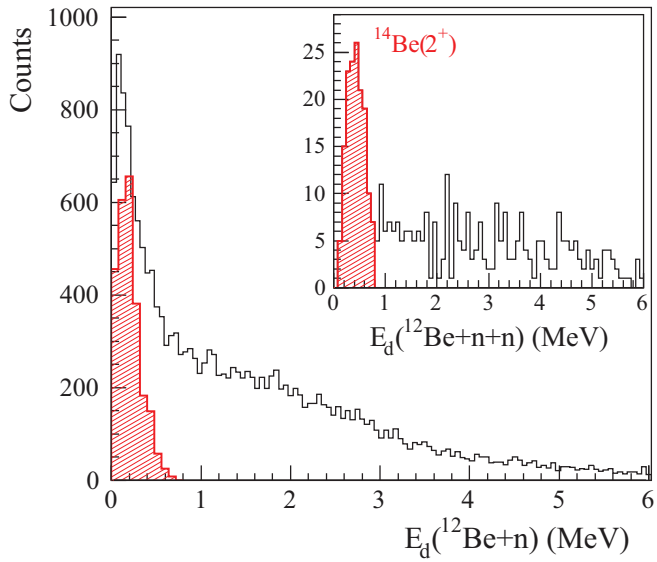

FIG. 9. (Color online) Reconstructed $^{12}\mathrm{Be}+n$ decay energy for the C(^{15}B,$^{12}\mathrm{Be}+n$) reaction. Inset: $^{12}\mathrm{Be}+n+n$ decay energy spectrum from the C(^{15}B,$^{12}\mathrm{Be}+n+n$) reaction. The hatched (red) distribution represents $^{12}\mathrm{Be}+n$ events, reconstructed from the $^{12}\mathrm{Be}+n+n$ data, arising from the decay of the $^{14}\mathrm{Be}(2^+_1)$ state (hatched events in the inset) and renormalized to account for the one- versus two-neutron detection efficiencies.

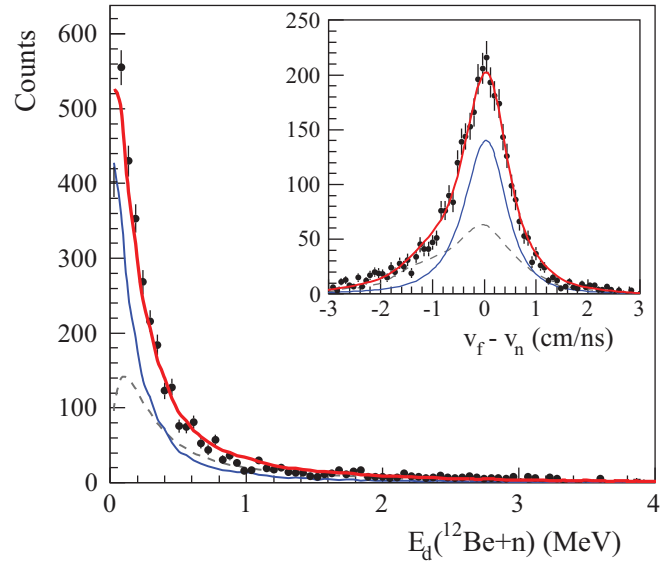

FIG. 10. (Color online) Reconstructed $^{12}\mathrm{Be}+n$ decay energy and relative velocity (inset) spectra from the C(^{15}B,$^{12}\mathrm{Be}+n$) reaction for neutrons with $\theta_{\mathrm{lab}} < 3^\circ$. Both the uncorrelated distribution [dashed (gray) line] and that representing an s-wave virtual state with $a_s = -10$ fm [lower (blue) solid line] are shown.

to ^{13}Be.[5] In the first case, the states in ^{13}Be are directly populated, while the character of any intermediate states in the second scenario will influence to some degree the $^{12}\mathrm{Be}+n$ decay energy spectrum. Such effects were evaluated here by analyzing the $^{12}\mathrm{Be}+n+n$ events.

The inset in Fig. 9 shows the reconstructed $^{12}\mathrm{Be}+n+n$ decay energy spectrum. As expected, the statistics are reduced with respect to the $^{12}\mathrm{Be}+n$ data owing to the lower two-neutron detection efficiency, which includes the cross-talk rejection (Sec. II). Nevertheless, the spectrum displays, in addition to a very broad nonresonant continuum, a prominent peak some 0.3 MeV above the two-neutron threshold which corresponds to the known $E_x = 1.5$ MeV 2^+_1 state of ^{14}Be [82]. Clearly, given the limited energy available for the decay of this state into $^{12}\mathrm{Be}+n+n$, $^{12}\mathrm{Be}+n$ events of an even lower average decay energy will be observed. Indeed, when the $^{12}\mathrm{Be}+n$ events are confined to those arising from the decay of $^{14}\mathrm{Be}(2^+)$—$E_{^{12}\mathrm{Be}+n+n} < 0.8$ MeV—they are seen, unsurprisingly, to constitute the very narrow structure at threshold (Fig. 9). That is, the threshold strength in the $^{12}\mathrm{Be}+n$ relative energy spectrum arises from the limited energy available in the decay of $^{14}\mathrm{Be}^*(2^+)$ populated in the proton removal from ^{15}B. Given that the form and threshold location of the peak are very close to those associated with a strongly interacting s-wave virtual state, it is very probable that the $^{12}\mathrm{Be}+n$ coincidence data from stable-beam fragmentation was dominated by the decay of $^{14}\mathrm{Be}(2^+)$ rather than direct population of ^{13}Be, as implicitly assumed in the analyses of these experiments [31,32]. The present work mirrors that of the earlier study by Kondo *et al.* [34], wherein the population of $^{14}\mathrm{Be}(2^+)$ in the dissociation of ^{14}Be was identified, also through the analysis of the $^{12}\mathrm{Be}+n+n$ events, as the source of the sharp threshold peak in the corresponding $^{12}\mathrm{Be}+n$ decay energy spectrum.

It is possible to proceed further and mock up the very restricted acceptances of the stable-beam studies by limiting the neutron detection in the present work to very forward angles ($\theta_n < 3^\circ$) and analyzing the resulting $^{12}\mathrm{Be}+n$ events. In Fig. 10 the results are shown for the $^{12}\mathrm{Be}+n$ decay energy and relative velocity, where the restricted acceptances privilege almost exclusively the peak at threshold produced by the decay of $^{14}\mathrm{Be}^*(2^+)$ and resemble very closely the Be(^{18}O,$^{12}\mathrm{Be}-n$) relative velocity spectrum in Ref. [31] and the Be(^{48}Ca,$^{12}\mathrm{Be}-n$) decay energy spectrum in Ref. [32].

To provide a more quantitative comparison, the restricted acceptance data set was used to generate uncorrelated $^{12}\mathrm{Be}-n$ distributions and the two spectra were then described using this distribution (which, as noted earlier, includes the experimental response) together with a virtual s-wave-state line shape that had been filtered through the simulation [60]. In order to make a direct comparison, the results are shown for the limit on the scattering length of –10 fm deduced in Ref. [31]. As may be seen, this description reproduces both spectra very well and reinforces the notion that the strongly interacting s-wave virtual state deduced from the stable-beam fragmentation studies was an artifact resulting from the population and decay of the $^{14}\mathrm{Be}(2^+)$ state. In the following, therefore, the discussion concentrates on the interpretation, in the light of theoretical considerations, of the C(^{14}B,$^{12}\mathrm{Be}+n$) decay energy spectrum.

[5]Owing to the very much higher (16 MeV) proton-versus-neutron separation energy in ^{14}B, neutron removal followed by proton decay is extremely unlikely.

IV. DISCUSSION

As noted earlier, single-proton removal from ^{14}B is expected to populate final states in ^{13}Be with neutron configurations corresponding to those of the valence neutron in the former; that is, $\nu 2s_{1/2}$ and $\nu 1d_{5/2}$ configurations. In this context (Sec. III A), the broad structure at 0.70 MeV may be identified as a $1/2^+$ state, and that at 2.40 MeV as $5/2^+$. In terms of the latter, the single-particle width for a d-wave resonance at this energy is $\Gamma_{sp} \approx 0.90$ MeV, compared to a measured width of 0.70 ± 0.32 MeV, suggesting a strong single-particle character. In a simple picture, where the ^{13}Be levels are essentially single particle ($^{12}\text{Be} \otimes \nu nlj$), yields reflecting the spectroscopic factors characterizing the initial state would be expected for proton removal [55]. After correcting for the detection efficiency and the contribution of the uncorrelated distribution, the structure centered around 0.70 MeV is seen to be populated 3.6 ± 0.8 times more strongly than that at 2.40 MeV, which may be compared to the ratio of 2.1 of the corresponding ^{14}B spectroscopic factors (Sec. III A). Finally, the separation between the two levels of 1.70 ± 0.18 MeV may be compared to the $1/2^+$–$5/2^+$ energy difference of some 2.3 MeV estimated [47] on the basis of a linear extrapolation of the corresponding levels in less exotic $N = 9$ isotones, in the spirit of Talmi and Unna [1], and the difference in the $\nu 2s_{1/2}$ and $\nu 1d_{5/2}$ effective single-particle energies of around 1.5 MeV in ^{14}B deduced from a very recent $d(^{13}\text{B},p)$ reaction study [18]. Interestingly, it may be noted that the lowering of the $\nu 2s_{1/2}$ orbital with respect to the $\nu 1d_{5/2}$ is expected in a simple potential [20] and is enhanced by weak binding [83], effects which have been revisited in a very recent study of the systematics of the $1/2^+$ and $5/2^+$ levels in light nuclei [84].

Given the mixed $(0+2)\hbar\omega$ character of ^{12}Be [5–7], it is clear that interpretations beyond the naive $^{12}\text{Be} \otimes \nu nlj$ description should be sought. In this context, Fortune [47] has estimated, within a simple model [85], the energies of the $^{10}\text{Be} \otimes (\nu 2s1d)^3_J$ levels, with particular focus on the corresponding $5/2^+$ state. The results are shown in Fig. 11, where it is assumed that the lowest $1/2^+$ level is 0.4 MeV above threshold, as proposed here (see below). The lowest-lying $5/2^+$ level, some 1.4 MeV above the $1/2^+$ $^{12}\text{Be} \otimes \nu 2s_{1/2}$ state, is $^{10}\text{Be} \otimes (\nu 2s1d)^3$, whereas the $5/2^+$ $^{12}\text{Be} \otimes \nu 1d_{5/2}$ level is, based on the estimated $1/2^+$–$5/2^+$ energy difference, higher-lying at 2.3 MeV. In terms of the interpretation of the present data, unless the $1/2^+$ state were to lie at threshold, the $5/2^+_2$ level is energetically permitted to decay via d-wave neutron emission to the isomeric $^{12}\text{Be}(0^+_2)$ level ($E_x = 2.24$ MeV), the decay of which could not be detected here. As noted by Fortune and Sherr [85], despite the low available decay energy, structural considerations suggest that decay to the isomeric state could possibly be favored (we return to this point below).

In order to explore in more detail the location and structure of the low-lying states of ^{13}Be, shell-model calculations within the s-p-sd-pf model space and employing the WBP interaction [86] have been undertaken. The calculations follow the same prescription as that in Ref. [87], whereby an additional psd energy-gap parameter (Δ_{spd}) was introduced to account for the mixing between the 0 and $2\hbar\omega$ and the 1 and $3\hbar\omega$ configurations [88]. Importantly, Δ_{spd} was chosen in order to reproduce the experimentally determined configuration mixing in the $^{12}\text{Be}_{gs}$ [6,7]. The resulting level scheme (up to 3 MeV) for ^{13}Be is displayed in Fig. 11, while the energies, spectroscopic factors for proton removal from ^{14}B, and those describing the structural overlap with states in ^{12}Be are listed in Table I.

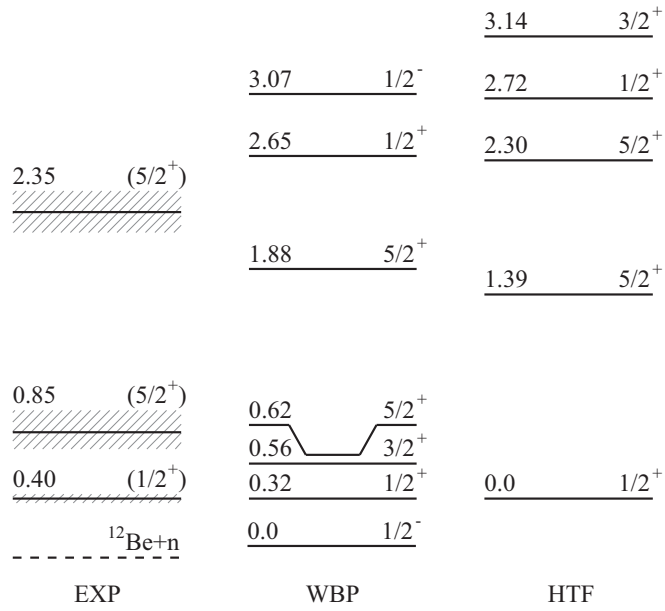

FIG. 11. Levels (MeV) in ^{13}Be as predicted by $(0-3)\hbar\omega$ shell-model calculations (WBP) and estimated, for positive-parity states, within the simplified scheme of Fortune (HTF) [47], where the lowest $1/2^+$ state is assumed to lie 0.4 MeV above threshold. These two level schemes are normalized to the predictions for the $1/2^+_1$ state, and the energies indicated are with respect to the lowest-lying level of each calculation. The results of the present work are also shown (EXP), where the level 0.40 MeV above the $^{12}\text{Be} + n$ threshold is identified with the predicted $1/2^+_1$ state. Experimental energies are listed with respect to the $^{12}\text{Be} + n$ threshold. Shaded bands represent the experimental uncertainties in the resonance energies (Table II).

While our interest here is primarily on the positive-parity states, it is interesting to note that the $1/2^-$ $1\hbar\omega$ $\nu 1p^{-1}_{3/2}$ level is predicted to be the lowest-lying one, 0.32 MeV below the $1/2^+_1$ state. The first $5/2^+$ level, with a $2\hbar\omega$ $^{10}\text{Be} \otimes (\nu 2s1d)^3$ parentage, is found at 0.62 MeV, in close proximity to the $3/2^+$ level with the same parentage. The second $5/2^+$ level, with a $0\hbar\omega$ $^{12}\text{Be} \otimes (\nu 1d_{5/2})$ parentage, is predicted to lie 1.88 MeV above the $1/2^-$, implying a $1/2^+$–$5/2^+$ energy difference of 1.56 MeV—smaller than that based on the extrapolation from less exotic $N = 9$ isotones. Interestingly, in unmixed calculations the $5/2^+$ 0 and $2\hbar\omega$ levels are degenerate and the $0\hbar\omega$ $1/2^+$ state lies only around 0.7 MeV below and is separated by 1.7 MeV from its higher-lying $2\hbar\omega$ counterpart [89].

The most strongly populated states in single-proton removal from ^{14}B are predicted (Table I) to be the $1/2^+_1$ ($C^2S = 0.41$) and $5/2^+_2$ states ($C^2S = 0.43$), while the $5/2^+_1$ level is predicted to carry a factor 3 less strength ($C^2S = 0.13$). The remaining strength—less than 5% of the total lying below

TABLE I. Low-lying level structure of ^{13}Be predicted by $(0-3)\hbar\omega$ shell-model calculations using the WBP interaction [88] in the s-p-sd-fp valence space (see text). E_x is the excitation energy with respect to the $1/2^-_1$ state; C^2S is the spectroscopic factor for removing a $1p_{3/2}$ proton from ^{14}B; $b_{s/d}$ is the spectroscopic factor for s- or d-wave neutron decay to ^{12}Be$(0^+_1,2^+_1,0^+_2)$ for states with nonzero C^2S (values are listed even if the decay is not energetically possible).

J^π_i	E_x (MeV)	C^2S	$b_{s/d}$		
			^{12}Be(0^+_1)	^{12}Be(2^+_1)	^{12}Be(0^+_2)
$1/2^-_1$	0.0				
$1/2^+_1$	0.316	0.41	0.57(s)	0.05(d)	0.23(s)
$3/2^+_1$	0.562	0.00	0.04(d)	1.13(d)	0.01(d)
$5/2^+_1$	0.619	0.13	0.67(d)	0.08(s)/0.05(d)	<0.01
$5/2^+_2$	1.885	0.43	0.01(d)	0.23(s)/0.01(d)	0.65(d)
$1/2^+_2$	2.652	0.05	0.05(s)	0.33(d)	0.35(s)
$1/2^-_2$	3.069				

the two-neutron emission threshold—is carried by the $1/2^+_2$ level ($C^2S = 0.05$). As the $3/2^+$ $2\hbar\omega$ state does not have a corresponding $0\hbar\omega$ level to mix with, it will be only very weakly populated in direct proton removal from ^{14}B. In the case of the $1/2^+$ states, the quite large separation permits only a relatively small amount of mixing to occur and hence a rather weak yield to the $1/2^+_2$ level.

In the light of these calculations, the description of the C(^{14}B,^{12}Be $+ n$) decay energy spectrum has been reappraised under the assumption of three states being appreciably populated: low-lying ($E_d \lesssim 1$ MeV) s- and d-wave levels together with a higher-lying ($E_d \sim 1.5$–3.0 MeV) d-wave resonance. As shown in Fig. 12, the spectrum is very well reproduced, including, in particular, the region below 1 MeV, which is composed of an s-wave resonance at 0.40 ± 0.03 MeV ($\Gamma_r = 0.80^{+0.18}_{-0.12}$ MeV) and a narrower d-wave resonance at $0.85^{+0.15}_{-0.11}$ MeV ($\Gamma_r = 0.30^{+0.34}_{-0.15}$ MeV), while the higher-lying d-wave resonance is at $E_r = 2.35 \pm 0.14$ MeV with a width $\Gamma_r = 1.50 \pm 0.40$ MeV (Table II and Fig. 11). The widths of the d-wave states may be compared to estimates of the corresponding single-particle widths of 0.08 and 0.90 MeV. We note that the experimental resolution (FWHM) at 0.85 MeV is ~380 keV, hence the uncertainty of the width of this level is rather large.

In terms of the yields to the three levels, the shell-model calculations indicate, normalizing the $1/2^+$ to a strength of 1.00, that the $5/2^+_1$ and $5/2^+_2$ states should be populated with strengths of 0.32 and 1.05. Experimentally, strengths of 0.40 ± 0.07 ($5/2^+_1$) and 0.80 ± 0.09 ($5/2^+_2$) are observed with respect to the $1/2^+$ level (Table II), in reasonably good agreement with the shell-model calculations.

TABLE II. Deduced J^π assignments, resonance energies (E_r) above the ^{12}Be $+ n$ threshold, widths (Γ_r), and strengths with respect to the $1/2^+$ level, for the adjustment to the data shown in Fig. 12.

J^π	E_r (MeV)	Γ_r (MeV)	$I/I(1/2^+)$
$1/2^+$	0.40 ± 0.03	$0.80^{+0.18}_{-0.12}$	1.00
$5/2^+$	$0.85^{+0.15}_{-0.11}$	$0.30^{+0.34}_{-0.15}$	0.40 ± 0.07
$5/2^+$	2.35 ± 0.14	1.50 ± 0.40	0.80 ± 0.09

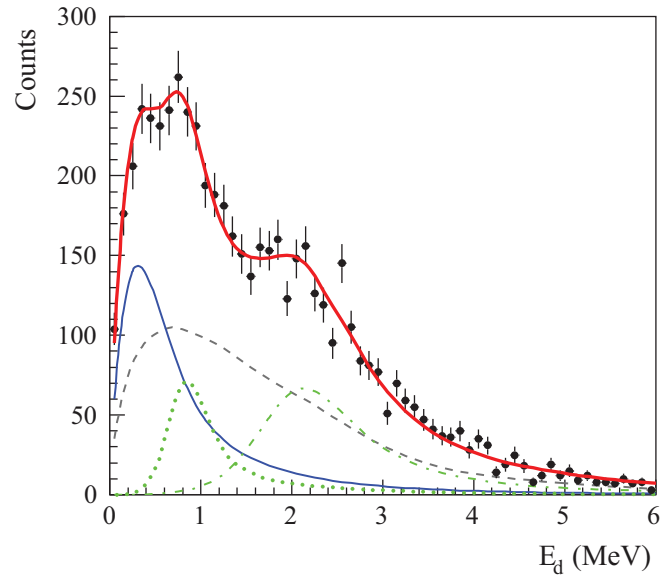

FIG. 12. (Color online) Reconstructed ^{12}Be $+ n$ decay energy for the C(^{14}B,^{12}Be $+ n$) reaction compared to simulations incorporating low-lying s [lower (blue) solid line] and d-wave resonances [dotted (green) line] and a higher-lying d-wave resonance [dot-dashed (green) line] together with a nonresonant continuum [dashed (gray) line].

Energetically, only the level at 2.35 MeV may decay to excited states in ^{12}Be (we ignore the possible small yield to the $1/2^+_2$ level) rather than only directly to the ground state. In the case of decay to the isomeric 2.25 MeV ^{12}Be(0^+_2) state, this can only occur for the high-energy side of the 2.35 MeV resonance and, despite the large structural overlap (Table I), will be very strongly suppressed by the very low effective decay energy. Decay to the 2.11-MeV ^{12}Be(2^+_1) state is slightly more favorable, as energetically a larger fraction of the resonance can decay via this pathway. Structurally there is a significant overlap for decay via s-wave neutron emission to ^{12}Be(2^+_1), and while the decay to the ^{12}Be$_{gs}$ is energetically greatly favored, it is structurally very strongly suppressed (Table I). Experimentally, however, no indication was found here (Sec. III A) for a significant yield to ^{12}Be(2^+_1). In addition, from a practical point of view any low-energy decays to ^{12}Be(2^+_1) [or ^{12}Be(0^+_2)] would need to be quite strong and narrow to be identified at threshold in the decay energy spectrum. We note that if the energy of the proposed $5/2^+_2$ level is at the lower bounds of the present uncertainties, then the fraction of the distribution energetically allowed to decay via neutron emission to the ^{12}Be(2^+_1) state would be greatly reduced. Alternatively, or in addition, it is possible that the structural overlap between the $5/2^+_2$ level and the ^{12}Be(2^+_1) state is overestimated by the shell model.

In closing this discussion, we turn to a comparison with recent work which has employed the complementary probe of neutron removal from ^{14}Be [22,34,45]. The results of these

studies have been enumerated in Sec. I and are displayed in Fig. 13 together with the results of the present work. As observed in Ref. [45], while the decay energy spectra are similar—a well-populated peak-like structure centered below 1 MeV, with a less-well-defined feature at higher energies (∼2–3 MeV)—the interpretations are at variance.

Both the present study and the latest neutron knockout work [45] agree that the low-energy region of the decay energy spectra is dominated by resonant s-wave strength rather than the weakly interacting virtual s-wave strength invoked earlier [22,34]. While Ref. [45] employed the contention of our earlier ^{14}B proton-removal study of a broad low-lying s-wave resonance [36] (explored here in Sec. IIIA and Fig. 8) as initial input to their analysis, the dominance of the s-wave strength was confirmed by the $^{12}\mathrm{Be}+n$ "profile" function (transverse momentum distribution as a function of decay energy) [37,45]. In contrast, the intermediate energy measurement [34] identified the low-lying peak as an $\ell = 1$ resonance based on the associated $^{12}\mathrm{Be}+n$ transverse momentum distribution. The strength—almost 50% of the total measured yield—is somewhat surprising given that the ^{14}Be wave function is believed to be dominated by $\nu 2s^2_{1/2}$ and $\nu 1d^2_{5/2}$ valence neutron configurations [10,21]. It may be noted that the form of the decay energy spectrum near threshold in this measurement is dependent on the subtraction of the narrow component arising from the population and decay of the $^{14}\mathrm{Be}(2^+_1)$ (Sec. III B).

In terms of s-wave strength, it was also proposed [45], following structural considerations similar to those of Fortune [47] discussed above (Fig. 11), that a second higher-lying $1/2^+$ (2.9 MeV) is populated in the high-energy neutron removal. While difficult to identify directly in the decay energy spectrum owing to its very broad width ($\Gamma \approx 4$ MeV), its presence was argued for on the basis of the influence on the line shape of the combined s-wave strength. Here, as noted earlier, in proton removal from ^{14}B, the $1/2^+_2$—predicted by the shell model at around 2.7 MeV[6]—is expected to be only relatively weakly populated (Table I), whereas the identification of such a state in the present data would require a significant yield to it given the intrinsically very broad width and the proximity of the 2.35-MeV level.

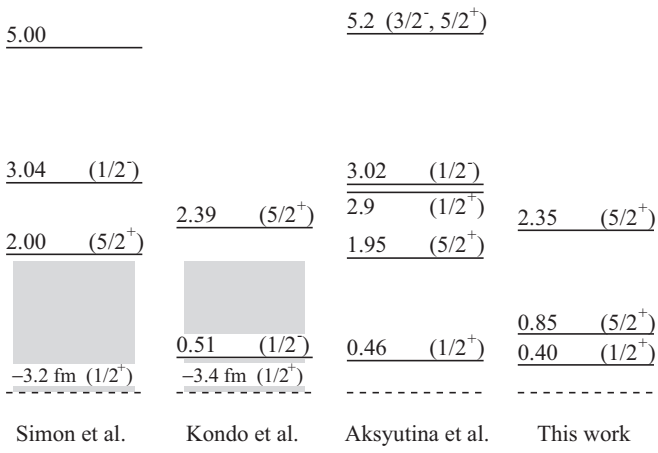

FIG. 13. Comparison of the present work with the neutron removal studies by Simon *et al.* [22], Kondo *et al.* [34], and Aksyutina *et al.* [45]. Energies of the levels (MeV) with respect to the $^{12}\mathrm{Be}+n$ threshold (dashed line) are shown, together with the proposed spin-parity assignments. In the case of Refs. [22] and [34] the weakly interacting virtual s-wave strength is indicated by the gray bands and the corresponding scattering lengths are noted.

Turning to the d-wave strength, all of the studies agree on its presence in the region of ∼2–2.5 MeV. While the present investigation and that of Kondo *et al.* [34] concur on the energy of the corresponding $5/2^+$ level, the high-energy neutron removal studies, guided by the heavy-ion multinucleon transfer and pion absorption experiments [28–30,38], place it around 0.4 MeV lower [22,45]. In contrast, none of the neutron removal studies observe any clear evidence of a low-lying $5/2^+$ level, such as that deduced in the present work. Reference [45], however, suggested, based on the profile function, the possibility that an $\ell > 0$ resonance might exist at around 1 MeV. Conceivably, depending on the detailed structure of ^{14}Be, such a state might be populated with much less strength than in the case of proton removal from ^{14}B.

Above 2.5 MeV, the present study and that in Ref. [34] see no clear evidence of any states (note that for levels above 3.17 and 3.67 MeV the $^{11}\mathrm{Be}+2n$ and $^{10}\mathrm{Be}+3n$ channels are open). The high-energy neutron knockout studies [22,45], however, propose levels at 3.0 and close to 5 MeV, as inferred from the multinucleon transfer and pion absorption experiments [29,30,38]. The former was assigned $1/2^-$ and the latter suggested to be $3/2^-$ or $5/2^+$ [45]. Experimentally these two levels are very broad and quite weakly populated and the presence of at least the 5-MeV level should probably be regarded as provisional.

In terms of p-wave strength, only the intermediate-energy neutron removal study claims to observe a low-lying ($E_r = 0.51$ MeV) $1/2^-$ resonance [34]. As noted, neither of the high-energy studies corroborates this result, while the present investigation should not populate p-wave strength in any appreciable manner. As argued in Sec. I, there is good evidence from multinucleon transfer reaction [30] and pion absorption [38] studies of the existence of a $1/2^-$ level at around 0.8 MeV. In addition, the shell-model calculations predict (Fig. 11 and Table I) that the $1/2^-_1$ level should appear at low energies. As such, it may be concluded that the lowest $1/2^+$ and $1/2^-$ levels lie close together below 1 MeV.

V. CONCLUSIONS

In summary, the low-lying structure of the neutron unbound system ^{13}Be has been explored via invariant mass spectroscopy of the beam velocity neutron and ^{12}Be charged fragments from reactions of intermediate-energy (35 MeV/nucleon) secondary beams of ^{14,15}B on a carbon target. In the case of the breakup of ^{15}B, a very sharp peak at threshold was observed in the $^{12}\mathrm{Be}+n$ decay energy spectrum. Analysis of the $^{12}\mathrm{Be}+n+n$ events demonstrated, in line with earlier work [34], that this resulted from the sequential decay of the unbound $^{14}\mathrm{Be}(2^+)$ state rather than a strongly interacting

[6]Assuming the $1/2^+_1$ level to lie at 0.40 MeV (Fig. 11).

s-wave virtual state in ^{13}Be as had been surmised in some earlier stable-beam fragmentation studies.

In the second measurement, single-proton removal from ^{14}B was investigated. In this case a broad low-lying structure some 0.7 MeV above the neutron decay threshold was observed in the $^{12}\mathrm{Be}+n$ decay energy spectrum, in addition to a less prominent feature at around 2.4 MeV. Based on the selectivity of the reaction, which should populate states in ^{13}Be with neutron configurations mirroring those of ^{14}B, and a comparison with $(0-3)\hbar\omega$ shell-model calculations, the low-lying structure was deduced probably to arise from $J^\pi = 1/2^+$ and $5/2^+$ resonances at 0.40 ± 0.03 and $0.85^{+0.15}_{-0.11}$ MeV above threshold. The higher-lying feature is believed to arise from a second broad $5/2^+$ level at 2.35 ± 0.14 MeV. Taken in conjunction with earlier studies and the shell-model calculations presented here, the results suggest that the lowest $1/2^+$ and $1/2^-$ levels lie relatively close together below 1 MeV.

A number of improvements are clearly possible in terms of the work presented here. First, a more granular neutron array would enable the resolution of the reconstructed $^{12}\mathrm{Be}+n$ decay energy to be improved and, thus, allow the presence of the two low-lying resonances to be put on a firmer footing. Second, the introduction of a dedicated γ-detection array with a good efficiency would allow any possible decays via the $^{12}\mathrm{Be}(2^+_1)$ state to be investigated in coincidence with the neutrons for even relatively weak decays. Unfortunately, improved coincident γ-ray detection will not eliminate the complications arising from possible decays via the isomeric $^{12}\mathrm{Be}(0^+_2)$ state. Finally, a realistic theoretical treatment of the reaction would be welcome, including the population of the nonresonant continuum. While this is not an easy task, some notable steps in this direction have already been taken (see, for example, Ref. [90]).

Ideally, neutron transfer onto ^{12}Be should be studied using the (d,p) reaction (in inverse kinematics), whereby no ambiguity will arise in the energies of the states populated, as they are derived from the energies and angles of the protons. Moreover, such an approach should, in principle, populate both positive- and negative-parity states with $^{12}\mathrm{Be}_{\mathrm{gs}} \otimes \nu nlj$ components. Such an experiment presents many challenges, not the least of which is the ^{12}Be beam, the energy of which must be relatively low (of the order of 5−10 MeV/nucleon) in order to provide for reasonable cross sections for the low-angular-momentum transfers of interest.

ACKNOWLEDGMENTS

The support provided by the technical staff of LPC and the LISE crew is gratefully acknowledged, as are the efforts of the GANIL cyclotron operations team for providing the primary beam. Enlightening exchanges with John Schiffer and John Millener are also acknowledged. We also express our appreciation for the vital contributions made by our late colleague and friend Jean-Marc Gautier to all the CHARISSA+DEMON experiments undertaken by our collaboration. This work has been supported in part by the European Community within the FP6 contract EURONS RII3–CT-2004-06065. B.A.B. acknowledges support from NSF grant PHY-1068217.

[1] I. Talmi and I. Unna, Phys. Rev. Lett. **4**, 469 (1960).
[2] W. von Oertzen, Z. Phys. A **357**, 355 (1997).
[3] M. Freer *et al.*, Phys. Rev. Lett. **96**, 042501 (2006).
[4] D. J. Millener *et al.*, Phys. Rev. C **28**, 497 (1983).
[5] F. C. Barker, J. Phys. G **2**, L45 (1976).
[6] A. Navin *et al.*, Phys. Rev. Lett. **85**, 266 (2000).
[7] S. D. Pain *et al.*, Phys. Rev. Lett. **96**, 032502 (2006).
[8] I. Tanihata *et al.*, Phys. Lett. B **206**, 592 (1988).
[9] E. Liatard *et al.*, Europhys. Lett. **13**, 401 (1990).
[10] T. Suzuki *et al.*, Nucl. Phys. A **658**, 313 (1999).
[11] A. G. Artukh *et al.*, Phys. Lett. B **33**, 407 (1970).
[12] J. D. Bowman *et al.*, Phys. Rev. Lett. **31**, 614 (1973).
[13] P. Descouvemont, Phys. Rev. C **52**, 704 (1995).
[14] I. J. Thompson and M. V. Zhukov, Phys. Rev. C **53**, 708 (1996).
[15] V. Guimarães *et al.*, Phys. Rev. C **61**, 064609 (2000).
[16] E. Sauvan *et al.*, Phys. Lett. B **491**, 1 (2000).
[17] E. Sauvan *et al.*, Phys. Rev. C **69**, 044603 (2004).
[18] S. Bedoor *et al.*, Phys. Rev. C **88**, 011304(R) (2013).
[19] J. D. Goss *et al.*, Phys. Rev. C **12**, 1730 (1975).
[20] D. J. Millener, Nucl. Phys. A **693**, 394 (2001).
[21] M. Labiche *et al.*, Phys. Rev. Lett. **86**, 600 (2001).
[22] H. Simon *et al.*, Nucl. Phys. A **791**, 267 (2007).
[23] S. Ilieva *et al.*, Nucl. Phys. A **875**, 8 (2012).
[24] H. Iwasaki *et al.*, Phys. Lett. B **481**, 7 (2000).
[25] M. Labiche *et al.*, Phys. Rev. C **60**, 027303 (1999).
[26] G. Blanchon *et al.*, Phys. Rev. C **82**, 034313 (2010).
[27] Y. Kanada-En'yo, Phys. Rev. C **85**, 044320 (2012).
[28] D. V. Aleksandrov *et al.*, Sov. J. Nucl. Phys. **37**, 474 (1983).
[29] A. N. Ostrowski *et al.*, Z. Phys. A **343**, 489 (1992).
[30] A. V. Belozyorov *et al.*, Nucl. Phys. A **636**, 419 (1998).
[31] M. Thoennessen *et al.*, Phys. Rev. C **63**, 014308 (2000).
[32] G. Christian *et al.*, Nucl. Phys. A **801**, 101 (2008).
[33] A. A. Korsheninnikov *et al.*, Phys. Lett. B **343**, 53 (1995).
[34] Y. Kondo *et al.*, Phys. Lett. B **690**, 245 (2010).
[35] F. M. Marqués *et al.*, Phys. Rev. C **64**, 061301(R) (2001).
[36] J.-L. Lecouey, Few-Body Syst. **34**, 21 (2004).
[37] Y. Aksyutina *et al.*, Phys. Lett. B **718**, 1309 (2013).
[38] M. Gornov *et al.*, Bull. Russ. Acad. Sci. Phys. **62**, 1781 (1998).
[39] D. M. Brink, Phys. Lett. B **40**, 37 (1972).
[40] W. N. Catford *et al.*, Nucl. Phys. A **503**, 263 (1989).
[41] H. G. Bohlen *et al.*, Z. Phys. A **344**, 381 (1993).
[42] B. M. Young *et al.*, Phys. Rev. C **49**, 279 (1994).
[43] J. A. Caggiano *et al.*, Phys. Rev. C **60**, 064322 (1999).
[44] B. A. Chernyshev *et al.*, Eur. Phys. J. A **49**, 1 (2013).
[45] Y. Aksyutina *et al.*, Phys. Rev. C **87**, 064316 (2013).
[46] N. A. F. M. Poppelier *et al.*, Phys. Lett. B **157**, 120 (1985).
[47] H. T. Fortune, Phys. Rev. C **87**, 014305 (2013).
[48] P. Descouvemont, Phys. Lett. B **331**, 271 (1994).
[49] J. C. Pacheco and N. Vinh Mau, Phys. Rev. C **65**, 044004 (2002).
[50] T. Tarutina *et al.*, Nucl. Phys. A **733**, 53 (2004).
[51] I. Hamamoto, Phys. Rev. C **77**, 054311 (2008).
[52] Zhongzhou Ren, Baoqiu Chen, Zhongyu Ma, and Gongou Xu, Z. Phys. A **357**, 137 (1997).

[53] M. Zinser *et al.*, Phys. Rev. Lett. **75**, 1719 (1995).
[54] L. Chen *et al.*, Phys. Lett. B **505**, 21 (2001).
[55] J.-L. Lecouey *et al.*, Phys. Lett. B **672**, 6 (2009).
[56] H. Al Falou *et al.*, J. Phys.: Conf. Ser. **312**, 092012 (2011)
[57] R. Anne *et al.*, Nucl. Instr. Meth. A **257**, 215 (1987).
[58] M. MacCormick *et al.*, GANIL Report 98-02 (1998).
[59] G. Randisi, Ph.D. thesis, Université de Caen, 2011; http://tel.archives-ouvertes.fr/tel-00656582.
[60] A. Leprince, Ph.D. thesis, Université de Caen, 2009; http://tel.archives-ouvertes.fr/tel-00451526.
[61] F. M. Marqués *et al.*, Phys. Lett. B **381**, 407 (1996).
[62] M. Moszyński *et al.*, Nucl. Instr. Meth. A **343**, 563 (1994).
[63] I. Tilquin *et al.*, Nucl. Instr. Meth. A **365**, 446 (1995).
[64] M. Labiche, Ph.D. thesis, Université de Caen, 1999.
[65] F. M. Marqués *et al.*, Phys. Lett. B **476**, 219 (2000).
[66] F. M. Marqués *et al.*, Nucl. Instr. Meth. A **450**, 109 (2000).
[67] J.-L. Lecouey, Ph.D. thesis, Université de Caen, 2002; http://tel.archives-ouvertes.fr/tel-00003117.
[68] T. Baumann, A. Spyrou, and M. Thoennessen, Rep. Prog. Phys. **75**, 036301 (2012).
[69] H. Al Falou, Ph.D. thesis, Université de Caen, 2007; http://tel.archives-ouvertes.fr/tel-00212214.
[70] D. R. Tilley *et al.*, Nucl. Phys. A **708**, 3 (2002).
[71] D. E. Alburger *et al.*, Phys. Rev. C **17**, 1525 (1978).
[72] S. Shimoura *et al.*, Phys. Lett. B **560**, 31 (2003).
[73] S. Shimoura *et al.*, Phys. Lett. B **654**, 87 (2007).
[74] G. F. Bertsch, K. Hencken, and H. Esbensen, Phys. Rev. C **57**, 1366 (1998).
[75] M. Thoennessen *et al.*, Phys. Rev. C **59**, 111 (1999).
[76] K. W. McVoy and P. V. Isacker, Nucl. Phys. A **576**, 157 (1994).
[77] A. E. S. Green, *Nuclear Physics* (McGraw–Hill, New York, 1955).
[78] J.-L. Lecouey, RELISH, unpublished computer code, 2006.
[79] C. Joachain, *Quantum Collision Theory* (North-Holland, Amsterdam, 1975).
[80] A. Bohr and B. Mottelson, *Nuclear Structure, Vol. I* (W. A. Benjamin, New York, 1969).
[81] K. W. McVoy, Nucl. Phys. A **115**, 481 (1968).
[82] T. Sugimoto *et al.*, Phys. Lett. B **654**, 160 (2007).
[83] I. Tanihata, J. Phys. G **22**, 157 (1996).
[84] C. R. Hoffman, B. P. Kay, and J. P. Schiffer, arXiv:1311.1556 [nucl-ex] (2013).
[85] H. T. Fortune and R. Sherr, Phys. Rev. C **82**, 064302 (2010).
[86] E. K. Warburton and B. A. Brown, Phys. Rev. C **46**, 923 (1992).
[87] R. Kanungo *et al.*, Phys. Lett. B **682**, 391 (2010).
[88] E. K. Warburton *et al.*, Phys. Lett. B **293**, 7 (1992).
[89] D. J. Millener (private communication).
[90] G. Blanchon *et al.*, Nucl. Phys. A **784**, 49 (2007).